without hypoglycemia or weight gain: a double-blind, randomized, controlled trial in Japanese patients with type 2 diabetes. *Diabetes Res Clin Pract* 2008; 81: 161–168.
43. Nonaka K, Kakikawa T, Sato A, *et al.* Efficacy and safety of sitagliptin monotherapy in Japanese patients with type 2 diabetes. *Diabetes Res Clin Pract* 2007; 79: 291–298.
44. Mitsui R, Fukushima M, Nishi Y, *et al.* Factors responsible for deteriorating glucose tolerance in newly diagnosed type 2 diabetes in Japanese men. *Metabolism* 2006; 55: 53–58.
45. Saxena R, Hivert M, Langenberg C, *et al.* Genetic variation in GIPR influences the glucose and insulin responses to an oral glucose challenge. *Nat Genet* 2010; 42: 142–148.

ORIGINAL ARTICLE

GLP-1 receptor agonist attenuates endoplasmic reticulum stress-mediated β-cell damage in Akita mice

Shunsuke Yamane[1], Yoshiyuki Hamamoto[2], Shin-ichi Harashima[1], Norio Harada[1], Akihiro Hamasaki[1], Kentaro Toyoda[1], Kazuyo Fujita[1], Erina Joo[1], Yutaka Seino[3], Nobuya Inagaki[1,4]*

ABSTRACT

Aims/Introduction: Endoplasmic reticulum (ER) stress is one of the contributing factors in the development of type 2 diabetes. To investigate the cytoprotective effect of glucagon-like peptide 1 receptor (GLP-1R) signaling *in vivo*, we examined the action of exendin-4 (Ex-4), a potent GLP-1R agonist, on β-cell apoptosis in Akita mice, an animal model of ER stress-mediated diabetes.

Materials and Methods: Ex-4, phosphate-buffered saline (PBS) or phlorizin were injected intraperitoneally twice a day from 3 to 5 weeks-of-age. We evaluated the changes in blood glucose levels, bodyweights, and pancreatic insulin-positive area and number of islets. The effect of Ex-4 on the numbers of C/EBP-homologous protein (CHOP)-, TdT-mediated dUTP-biotin nick-end labeling (TUNEL)- or proliferating cell nuclear antigen-positive β-cells were also evaluated.

Results: Ex-4 significantly reduced blood glucose levels and increased both the insulin-positive area and the number of islets compared with PBS-treated mice. In contrast, there was no significant difference in the insulin-positive area between PBS-treated mice and phlorizin-treated mice, in which blood glucose levels were controlled similarly to those in Ex-4-treated mice. Furthermore, treatment of Akita mice with Ex-4 resulted in a significant decrease in the number of CHOP-positive β-cells and TUNEL-positive β-cells, and in CHOP mRNA levels in β-cells, but there was no significant difference between the PBS-treated group and the phlorizin-treated group. Proliferating cell nuclear antigen staining showed no significant difference among the three groups in proliferation of β-cells.

Conclusions: These data suggest that Ex-4 treatment can attenuate ER stress-mediated β-cell damage, mainly through a reduction of apoptotic cell death that is independent of lowered blood glucose levels. (J Diabetes Invest, doi: 10.1111/j.2040-1124.2010.00075.x, 2011)

KEY WORDS: Apoptosis, Endoplasmic reticulum stress, Glucagon-like peptide-1

INTRODUCTION

Type 2 diabetes is a chronic metabolic disorder characterized by the loss of β-cell function and mass. The mechanisms underlying the loss of β-cell function and mass are not fully understood, but recent studies have shown that endoplasmic reticulum (ER) stress is one of the causes of β-cell damage in diabetes[1]. Owing to increased demand for insulin secretion, β-cells show a highly developed ER[1]. The ER has a number of important functions, such as post-translational modification, folding and assembly of newly synthesized secretory proteins[2–4]. Thus, the ER plays an essential role in cell survival. ER function can be impaired by various conditions, including inhibition of protein glycosylation, reduction in formation of disulfide bonds, calcium depletion from the ER lumen, impairment of protein transport from the ER to the Golgi and expression of malfolded proteins[1]. Various physiological or pathological conditions that compromise ER functions are collectively termed ER stress[1–3]. To alleviate ER stress and promote cell survival, an adaptive response, known as unfolded protein response (UPR) is activated. UPR comprises translational attenuation, induction of chaperones and ER stress-associated degradation (ERAD). However, prolonged activation of UPR can ultimately lead to cell death by apoptosis.

Increased demand for insulin secretion under certain conditions, such as chronic hyperglycemia, might result in β-cell overload. Chronic hyperglycemia in diabetes can therefore induce persistent ER stress, cause β-cell dysfunction and finally lead to a reduction in β-cell mass through apoptosis[1].

Glucagon-like peptide 1 (GLP-1) is a physiological incretin, an intestinal hormone released in response to nutrient

[1]Department of Diabetes and Clinical Nutrition, Graduate School of Medicine, Kyoto University, [4]CREST of Japan Science and Technology (JST), Kyoto, [2]Center for Diabetes and Endocrinology, Tazuke Kofukai Medical Research Institute, Kitano Hospital, and [3]Division of Diabetes, Clinical Nutrition and Endocrinology, Department of Medicine, Kansai Electric Power Hospital, Osaka, Japan
*Corresponding author. Nobuya Inagaki Tel.: +81 75 751 3562 Fax: +81 75 771 6601
E-mail address: inagaki@metab.kuhp.kyoto-u.ac.jp
Received 21 July 2010; revised 25 August 2010; accepted 8 September 2010

ingestion that stimulates glucose-dependent insulin secretion. A growing body of evidence suggests that GLP-1 not only increases insulin secretion and upregulates insulin biosynthesis, but also stimulates β-cell proliferation and neogenesis[5–9], and inhibits β-cell apoptosis[9–16], resulting in increased β-cell mass. However, demonstration of an *in vivo* effect in the animal models of type 2 diabetes is problematic, because enhancement of GLP-1R signaling lowers blood glucose levels as result of its insulinotropic action, and it is difficult to evaluate the direct cytoprotective effects of GLP-1 in conditions of similar glucose toxicity.

In the present study, we investigated the cytoprotective effect of GLP-1R signaling *in vivo* on ER stress-mediated apoptotic cell death by using Akita mice, an animal model of ER stress-mediated diabetes mellitus. Akita mice have a point mutation in the insulin 2 gene, resulting in misfolding of insulin that leads to severe ER stress[17,18]. To exclude the possibility that the effect of Ex-4 on β-cells is mediated through improved blood glucose levels, we used three groups of mice: Akita mice treated with phosphate-buffered saline (PBS), Ex-4, or the sodium-coupled glucose transporter inhibitor phlorizin, which decreases blood glucose levels without increasing insulin secretion.

MATERIALS AND METHODS

Experimental Animals

Male C57BL/6 mice and male Akita mice were obtained from Shimizu (Kyoto, Japan). The animals were housed under a light/dark cycle of 12 h with free access to food and water. All experiments were approved by the Kyoto University Animal Care Committee.

In vivo Treatment

The mice were given twice daily intraperitoneal injections of PBS, Ex-4 (24 nmol/kg) or phlorizin (0.3 g/kg) for 2 weeks (from 3 to 5 weeks-of-age). Blood glucose levels were measured every third day by enzyme electrode method using a portable glucose analyzer (Glutest sensor; Sanwakagaku, Nagoya, Japan). Blood samples were collected from tail cuttings from these mice fed *ad libitum*. At the end of the experimental period, blood samples were collected from the inferior vena cava under anesthesia to determine the plasma glycoalbumin levels (Oriental Yeast, Tokyo, Japan). Pancreas samples from each of the animal groups were obtained for histological evaluation, and islets were isolated for measurement of insulin content and RNA extraction.

Evaluation of Pancreatic Insulin-Positive Area and Number of Islets

The pancreas samples were fixed in Bouin's solution. Serial 5-μm paraffin-embedded tissue sections were mounted on slides. After rehydration, sections were incubated with polyclonal rabbit anti-insulin antibodies (Santa Cruz Biotechnology, Santa Cruz, CA, USA), with a biotinylated goat anti-rabbit antibody (DAKO, Carpinteria, CA, USA), and then with a streptavidin peroxidase conjugate and substrate kit (DAKO) using standard protocols. The total pancreas area and insulin-positive area were quantified on five distal, random, non-overlapping sections from five mice of each group using a BZ-8100 microscope equipped with a BZ-Analyzer (KeyEnce, Osaka, Japan). Insulin-positive areas and the number of islets of each group were adjusted by total pancreas area[15].

Measurement of Insulin Contents of Isolated Islets

Pancreatic islets were isolated by collagenase digestion. To determine insulin contents, islets were homogenized in 400 μL acid ethanol (37% HCl in 75% ethanol, 15:1000 [v/v]) and extracted at 4°C overnight. The acidic extracts were dried by vacuum, reconstituted and subjected to insulin measurement. The amount of immunoreactive insulin was determined by radioimmunoassay (RIA).

Measurement of mRNA Expression of C/EBP-Homologous Protein and BiP in Isolated Islets

Measurement of mRNA expression of C/EBP-homologous protein (CHOP) and BiP was carried out by quantitative reverse transcription polymerase chain reaction (RT–PCR) as described previously[19]. Briefly, total RNA was extracted from isolated islets with an RNeasy mini kit (Qiagen, Valencia, CA, USA) and treated with DNase (Qiagen). cDNA was prepared by SuperScript Reverse Transcriptase system (Invitrogens, Carlsbad, CA, USA) according to the manufacturer's instructions. CHOP mRNA levels and BiP mRNA levels in the islets were measured by quantitative RT–PCR using an ABI PRISM 7000 Sequence Detection System (Applied Biosystems, Foster City, CA, USA). The sequences of forward and reverse primers to evaluate

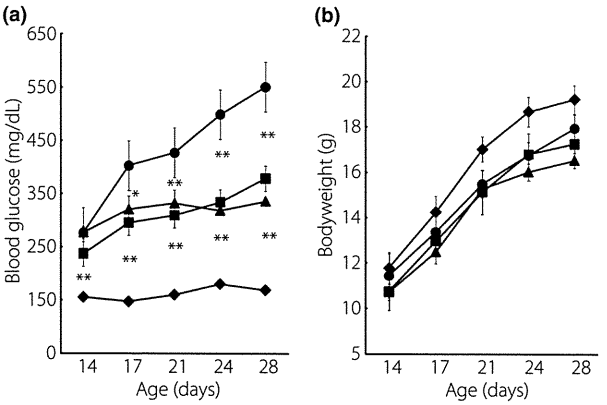

Figure 1 | Ex-4 significantly reduced blood glucose levels in Akita mice. (a) Blood glucose concentration and (b) bodyweight were measured in wild-type C56BL/6 mice (closed diamond, $n = 10$), Akita mice treated with PBS alone (closed circle, $n = 10$), Ex-4 (closed square, $n = 12$) and phlorizin (closed triangle, $n = 10$). Each symbol represents mean ± SE. $^{*}P < 0.05$, $^{**}P < 0.01$ *vs* PBS-treated Akita mice.

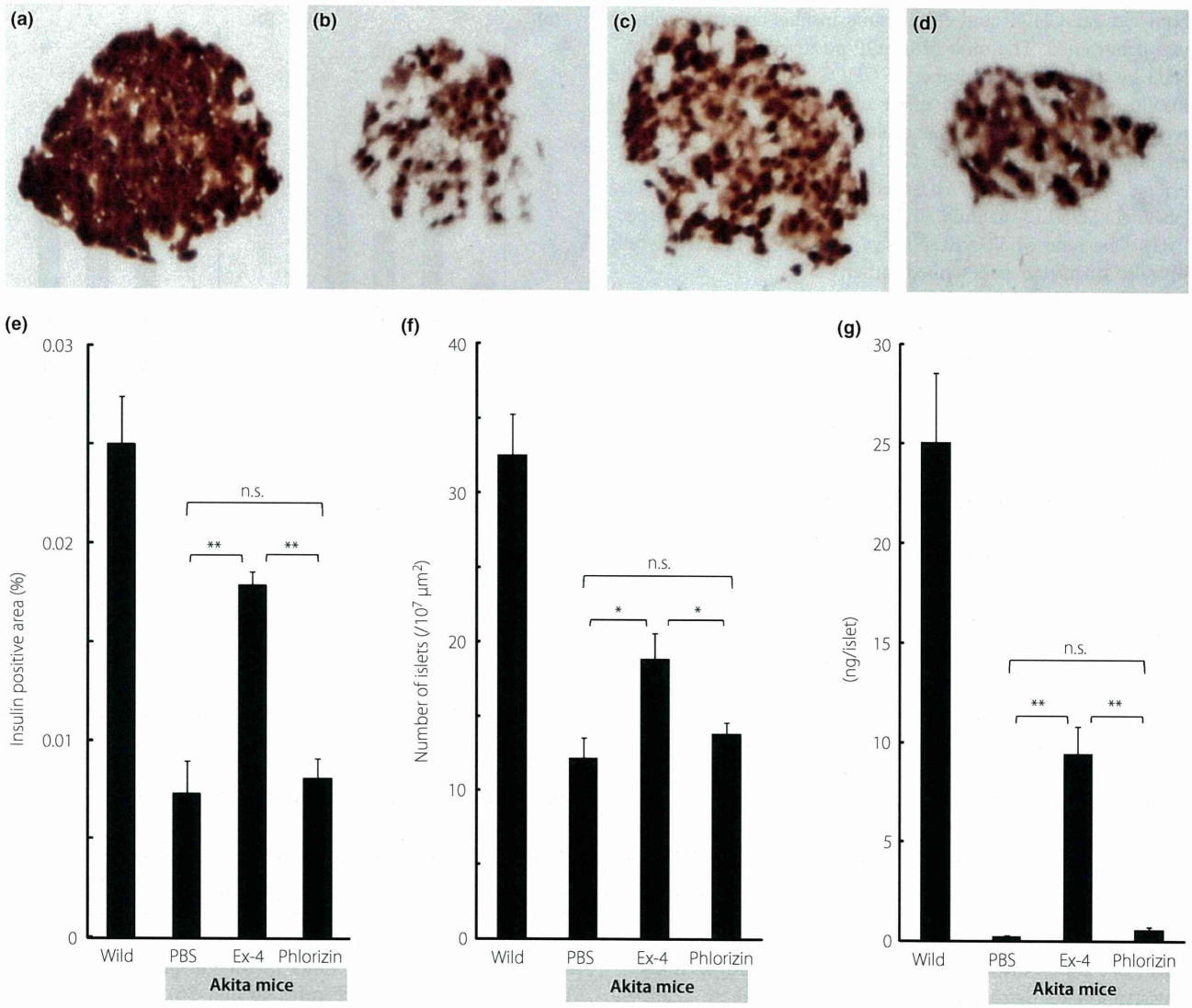

Figure 2 | Ex-4 treatment increased insulin-positive areas, number of islets and insulin content. (a–d) Representative mouse pancreata at 5 weeks-of-age stained with insulin. (a) Wild, (b) Akita mice treated with PBS, (c) Ex-4 or (d) phlorizin. (e) Insulin-positive areas and (f) number of islets were evaluated as described in Materials and Methods (n = 5 for each group). (g) Pancreatic insulin content was measured as described in Materials and Methods, and expressed as ng/islet (n = 5 for each group). Each column represents mean ± SE. *P < 0.05, **P < 0.01.

CHOP expression were 5′-GAGCT- GGAAGCCTGGTATGA-3′ and 5′-GGACGCAGGGTCAAGAGTAG-3′, respectively; the sequences of forward and reverse primers to evaluate BiP expression were 5′-TTTCTGCCATGGTTCTCACTAA-3′ and 5′-GCTGGGCATCATTGAAGTAAG-3′, respectively; and the sequences of forward and reverse primers to evaluate glyceraldehyde 3-phosphate dehydrogenase (GAPDH) expression were 5′-AGCTCACTGGCATGGCTTCCG-3′ and 5′-GCCTGCTTC-ACCACCTTCTTGATG-3′, respectively. SYBER Green PCR Master Mix (Applied Biosystems) was prepared for the PCR run. Thermal cycling conditions were denatured at 95°C for 10 min followed by 50 cycles at 95°C for 15 s and 60°C for 1 min. Total CHOP and total BiP levels were corrected by GAPDH mRNA levels.

Immunofluorescence Staining

For pancreatic CHOP and insulin immunohistochemistry, the tissues were fixed and embedded in paraffin. Serial 5-μm sections were stained with anti-CHOP/GADD153 (Santa Cruz Biotechnology) and anti-insulin (DAKO) antibodies using standard protocols. Insulin immunopositive areas were measured on five distal, random, non-overlapping sections from five mice of each group using a BZ-8100 fluorescence microscope equipped with a BZ-Analyzer (KeyEnce), and the number of cells showing

both nuclear CHOP and cytoplasmic insulin immunopositivity was determined. The ratio of CHOP-positive β-cells was calculated by adjusting the number of CHOP-positive β-cells by the insulin-positive area[20]. The effect of Ex-4 treatment on β-cell replication and apoptosis was evaluated histologically by proliferating cell nuclear antigen (PCNA) staining (Abcam, Cambridge, MA, USA) and TdT-mediated dUTP-biotin nick-end labeling (TUNEL) staining (Takara Bio, Otsu, Japan), respectively. The ratio of TUNEL-positive and PCNA-positive β-cells was also calculated as described earlier.

Statistical Analysis

Data are presented as means ± SEM. Statistical analyses were carried out by unpaired *t*-test. A *P*-value of <0.05 was considered significant.

RESULTS

Effect of Ex-4 on Hyperglycemia and Bodyweight in Akita Mice

Akita mice showed acute and progressive hyperglycemia at 14 days after birth and thereafter. Twice-daily intraperitoneal injection of Ex-4 from 3 to 5 weeks-of-age significantly reduced blood glucose levels compared with those in PBS-treated mice (Figure 1a). Plasma glucose levels in phlorizin-treated Akita mice were similar to those in Ex-4-treated mice. Plasma glycoalbumin levels were significantly lower in the Ex-4- and phlorizin-treated groups than those in the PBS-treated group, but no significant difference was observed between the Ex-4- and phlorizin-treated groups (12.9 ± 1.5 *vs* 8.7 ± 0.7 *vs* 8.2 ± 0.6, respectively, n = 10–12). Ex-4 treatment or phlorizin treatment did not change bodyweight compared with PBS treatment (Figure 1b). Ex-4 or phlorizin treatment did not change the amount of food intake assessed at 4 weeks-of-age (data not shown).

Effect of Ex-4 on Insulin-Positive Area and Number of Islets

Preservation of β-cell morphology was observed by treatment with Ex-4, as shown in Figure 2a. Quantitative histological analyses showed that Ex-4 treatment significantly increased both the insulin-positive area and the number of islets, whereas there was no significant difference between the PBS-treated group and the phlorizin-treated group (Figure 2b,c).

Effect of Ex-4 on Pancreatic Insulin Content

Figure 2d shows the effect of Ex-4 treatment on insulin content in pancreatic islets. Treatment with Ex-4 significantly increased insulin content in isolated islets, but phlorizin treatment did not.

Quantitative Estimation of CHOP and BiP Expression Levels by Real-Time PCR

The expression levels of CHOP mRNA are shown in Figure 3a, and those of BiP mRNA are shown in Figure 3b. Ex-4 significantly lowered the expression levels of CHOP and BiP mRNA, but there was no significant difference in the expression levels of CHOP or BiP mRNA between the phlorizin- or PBS-treated groups.

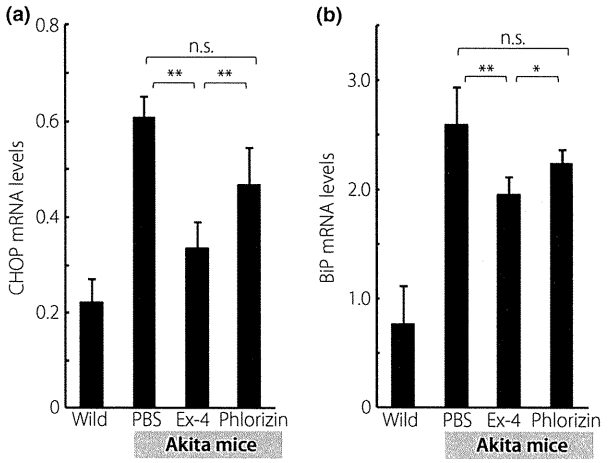

Figure 3 | Ex-4 treatment resulted in a significant decrease in the expression levels of C/EBP-homologous protein (CHOP) mRNA and Bip mRNA in Akita mice. (a) mRNA expression levels of CHOP were evaluated by quantitative real-time polymerase chain reaction (PCR). (b) mRNA expression levels of BiP were evaluated by quantitative real-time PCR. Data are expressed as the ratio to that of glyceraldehyde 3-phosphate dehydrogenase in the same sample (n = 5 for each group). Each column represents mean ± SE. *P < 0.05, **P < 0.01.

Effect of Ex-4 on the Ratio of CHOP-, TUNEL- and PCNA-Positive β-cells

Figure 4a depicts the representative pancreata stained with insulin (red), CHOP (green) and DAPI (blue), respectively. Similarly, Figure 5a shows the representative pancreata stained with insulin (red) and TUNEL (green). Treatment with Ex-4 significantly decreased the ratio of CHOP-positive β-cells and TUNEL-positive β-cells (Figures 4b and 5b), but there was no significant difference in the ratio of CHOP-positive or TUNEL-positive β-cells between the PBS- and phlorizin-treated groups. Figure 6a shows the representative pancreata stained with insulin (red) and PCNA (green). PCNA staining showed no significant difference in proliferation of β-cells among the three groups of Akita mice (Figure 6b). Interestingly, the ratio of PCNA-positive β-cells was increased in all three groups when compared with wild-type C57BL/6 mice.

DISCUSSION

Akita mice are widely used as an animal model of ER stress-mediated diabetes. Akita mice have a point mutation (C96T) in the insulin 2 gene[21] that disrupts the disulfide bond formation between the A and B chains of proinsulin, resulting in a drastic conformational change of the molecule. The unfolded proinsulin accumulates to the ER, causing severe ER stress leading to β-cell apoptosis. In humans, it has recently been shown that a mutation in the insulin gene, which is identical

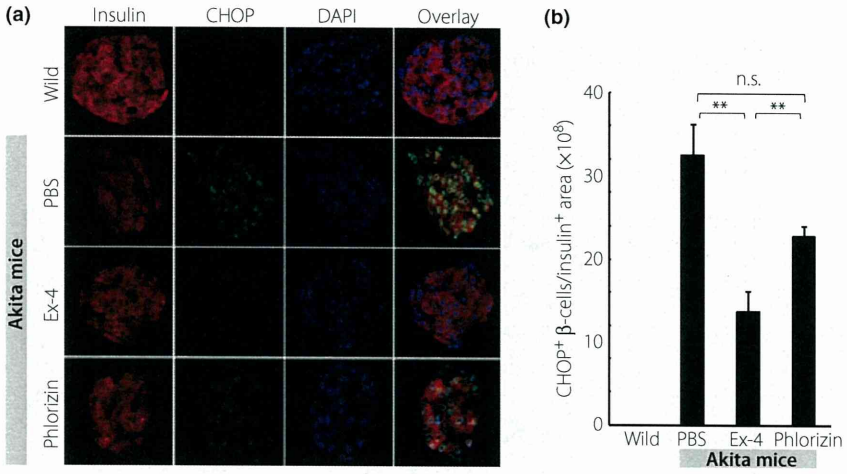

Figure 4 | Ex-4 treatment resulted in a significant decrease in the ratio of C/EBP-homologous protein (CHOP)-positive β-cells in Akita mice. (a) Representative mouse pancreata at 5 weeks-of-age stained with insulin (red), CHOP (green) and DAPI (blue). (b) The number of CHOP-positive β-cells normalized per insulin-positive area was quantified as described in Materials and Methods. Each column represents mean ± SE. $^{**}P < 0.01$.

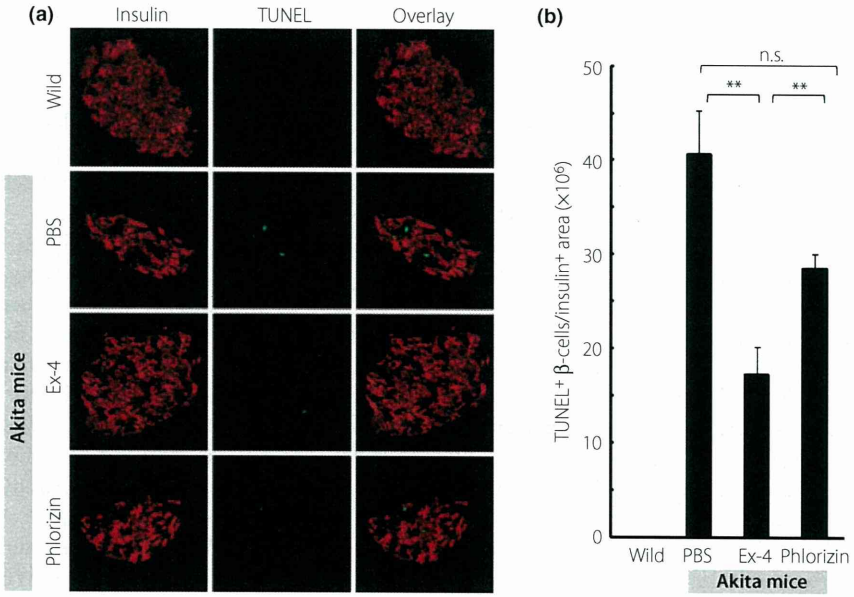

Figure 5 | Ex-4 treatment decreased the ratio of TUNEL-positive β-cells. (a) Representative mouse pancreata at 5 weeks-of-age stained with insulin (red) and TUNEL (green). (b) The number of TUNEL-positive β-cells normalized per insulin-positive area was quantified as described in Materials and Methods. Each column represents mean ± SE. $^{**}P < 0.01$.

to that in the Akita mouse, causes permanent neonatal diabetes within the first month of life that requires lifelong insulin injection[22].

In the present study, we have shown that Ex-4 treatment has a protective effect on β-cells in Akita mice. The insulin-positive area and the number of islets were maintained along with a decreased ratio of CHOP- and TUNEL-positive cells in the islets, showing that the major effect of Ex-4 treatment in the maintenance of β-cell mass is through decreasing β-cell apoptosis in response to ER stress. Because phlorizin decreases blood glucose levels without increasing insulin secretion, it might well reduce ER stress by decreasing the insulin demand. However, in contrast to the Ex-4 treatment, phlorizin treatment failed to show a reduction of ER stress or β-cell protective effects against

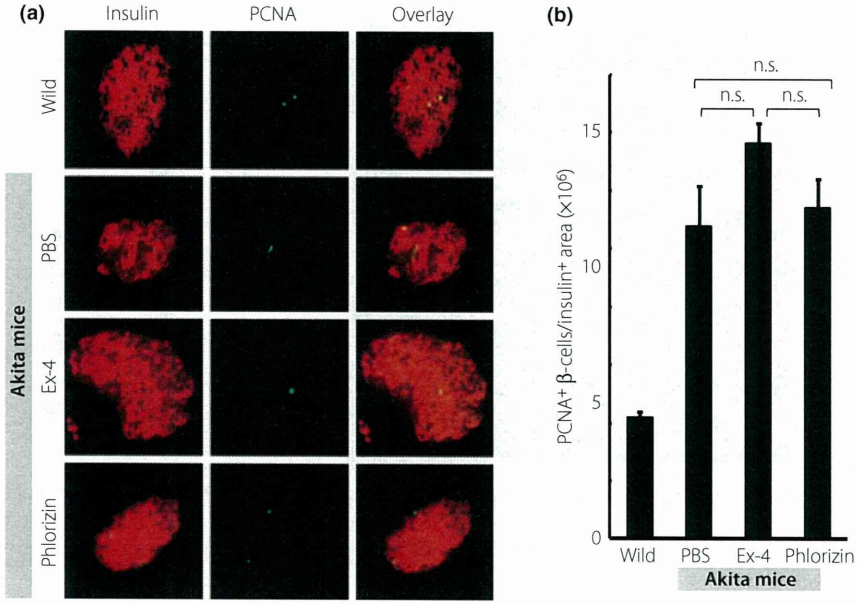

Figure 6 | Ex-4 treatment did not significantly increase the ratio of PCNA-positive β-cells. (a) Representative mouse pancreata at 5 weeks-of-age stained with insulin (red) and PCNA (green). (b) The number of PCNA-positive β-cells normalized per insulin-positive area was quantified as described in Materials and Methods. Each column represents mean ± SE.

apoptosis in our conditions. These findings show that Ex-4 has a direct effect on ER stress-mediated β-cell apoptosis that is independent of decreased insulin demand.

There are several *in vitro* and *in vivo* studies showing that GLP-1R agonists inhibit β-cell apoptosis[9–16], and several molecular mechanisms have been suggested. For example, GLP-1 treatment decreases the expression levels of proapoptotic protein caspase-3 and increases those of anti-apoptotic protein bcl-2 in isolated human islets[10]. It also has been shown that the anti-apoptotic effect of Ex-4 is associated with the activation of protein kinase B/Akt through PKA-dependent phosphorylation of CREB[11]. There are some reports that GLP-1 ameliorates ER stress. Yusta *et al.* found that treatment by Ex-4 reduces blood glucose levels in obese *db/db* mice along with a decrease in the number of CHOP-positive β-cells[20]. Tsunekawa *et al.*[23] reported a beneficial effect of Ex-4 on β-cell damage in calmodulin-over-expressing transgenic (CaMTg) mice that develop diabetes through ER stress-mediated β-cell apoptosis. They found that Ex-4 treatment reduced blood glucose levels while retaining the insulin-positive areas and decreasing the expression levels of CHOP mRNA in CaMTg mice. *In vitro* studies have found that rapid recovery from translational attenuation[19] or upregulation of BiP and JunB[24] accounts for the attenuation of ER stress-mediated β-cell damage by Ex-4 treatment. However, results of chronic Ex-4 treatment in animal models of type 2 diabetes should be carefully interpreted, because enhancement of GLP-1R signaling reduces the blood glucose level by its insulinotropic action. Therefore, the possibility remains that reduced hyperglycemia attenuates persistent ER stress and ameliorates β-cell apoptosis. Our present findings clearly show that Ex-4 treatment attenuates ER stress-mediated β-cell damage in Akita mice through a reduction of apoptotic cell death that is independent of decreased blood glucose levels.

Although several studies have found that the cytoprotective effect of GLP-1R signaling is not only through inhibition of β-cell apoptosis, but also through stimulation of β-cell proliferation[5–9], we did not find any effect of Ex-4 treatment on β-cell proliferation. It is possible that the administration period in the present study was too short to observe β-cell proliferation by Ex-4 or that stimulation of β-cell proliferation does not play a significant role in the cytoprotective effect of GLP-1R signaling in Akita mice. The ratio of PCNA-positive β-cells was increased not only in the Ex-4-treated group of Akita mice, but also in the phlorizin-treated group and the untreated group compared with that in wild-type C57BL/6 mice. Whether or not this result can be attributed to the phenotype of Akita mice requires further study.

Islet mass is reported to be decreased in patients with type 2 diabetes at the time of diagnosis[25]. Although Ex-4 is in clinical use for treatment of type 2 diabetes[26], superiority of Ex-4 over the other antidiabetic drugs has not been shown. Our data confirm the previous findings of a beneficial effect of Ex-4 on glycemic control, but also suggest that Ex-4 has a direct β-cell-protective effect independently of improved glycemic control. Thus, Ex-4 and other GLP-1R agonists might well be more effective than other antidiabetic drugs in clinical use in terms of alleviating β-cell damage and maintaining β-cell mass for diabetic patients.

ACKNOWLEDGEMENTS

This study was supported by Scientific Research Grants from the Ministry of Education, Culture, Sports, Science, and Technology of Japan, and from the Ministry of Health, Labor, Welfare, Japan, and by the Kyoto University Global COE Program 'Center for Frontier Medicine'. There is no conflict of interest for all the authors listed.

REFERENCES

1. Oyadomari S, Araki E, Mori M. Endoplasmic reticulum stress-mediated apoptosis in pancreatic β-cells. *Apoptosis* 2002; 7: 335–345.
2. Kaufman RJ. Stress signaling from the lumen of the endoplasmic reticulum: coordination of gene transcriptional and translational controls. *Genes Dev* 1999; 13: 1211–1233.
3. Mori K. Tripartite management of unfolded proteins in the endoplasmic reticulum. *Cell* 2000; 101: 451–454.
4. Kaufman RJ, Scheuner D, Schroder M, *et al.* The unfolded protein response in nutrient sensing and differentiation. *Nat Rev Mol Cell Biol* 2002; 3: 411–421.
5. Friedrichsen BN, Neubauer N, Lee YC, *et al.* Stimulation of pancreatic β-cell replication by incretins involves transcriptional induction of cyclin D1 via multiple signalling pathways. *J Endocrinol* 2006; 188: 481–492.
6. Miettinen P, Ormio P, Hakonen E, *et al.* EGF receptor in pancreatic β-cell mass regulation. *Biochem Soc Trans* 2008; 36: 280–285.
7. Jin T, Liu L. The Wnt signaling pathway effector TCF7L2 and type 2 diabetes mellitus. *Mol Endocrinol* 2008; 22: 2383–2392.
8. Zhou J, Pineyro MA, Wang X, *et al.* Exendin-4 differentiation of a human pancreatic duct cell line into endocrine cells: involvement of PDX-1 and HNF3β transcription factors. *J Cell Physiol* 2002; 192: 304–314.
9. Wang Q, Brubaker PL. Glucagon-like peptide-1 treatment delays the onset of diabetes in 8 week-old db/db mice. *Diabetologia* 2002; 45: 1263–1273.
10. Farilla L, Bulotta A, Hirshberg B, *et al.* Glucagon-like peptide 1 inhibits cell apoptosis and improves glucose responsiveness of freshly isolated human islets. *Endocrinology* 2003; 144: 5149–5158.
11. Jhala US, Canettieri G, Screaton RA, *et al.* cAMP promotes pancreatic β-cell survival via CREB-mediated induction of IRS2. *Genes Dev* 2003; 17: 1575–1580.
12. Li Y, Hansotia T, Yusta B, *et al.* Glucagon-like peptide-1 receptor signaling modulates β cell apoptosis. *J Biol Chem* 2003; 278: 471–478.
13. Buteau J, El Assaad W, Rhodes CJ, *et al.* Glucagon-like peptide-1 prevents beta cell glucolipotoxicity. *Diabetologia* 2004; 47: 806–815.
14. Bregenholt S, Moldrup A, Blume N, *et al.* The long-acting glucagon-like peptide-1 analogue, liraglutide, inhibits β-cell apoptosis *in vitro*. *Biochem Biophys Res Commun* 2005; 330: 577–584.
15. Park S, Dong X, Fisher TL, *et al.* Exendin-4 uses Irs2 signaling to mediate pancreatic β cell growth and function. *J Biol Chem* 2006; 281: 1159–1168.
16. Toyoda K, Okitsu T, Yamane S, *et al.* GLP-1 receptor signaling protects pancreatic beta cells in intraportal islet transplant by inhibiting apoptosis. *Biochem Biophys Res Commun* 2008; 367: 793–798.
17. Yoshioka M, Kayo T, Ikeda T, *et al.* A novel locus, Mody4, distal to D7Mit189 on chromosome 7 determines early-onset NIDDM in nonobese C57BL/6 (Akita) mutant mice. *Diabetes* 1997; 46: 887–894.
18. Oyadomari S, Koizumi A, Takeda K, *et al.* Targeted disruption of the Chop gene delays endoplasmic reticulum stress-mediated diabetes. *J Clin Invest* 2002; 109: 525–532.
19. Harada N, Yamada Y, Tsukiyama K, *et al.* A novel GIP receptor splice variant influences GIP sensitivity of pancreatic β-cells in obese mice. *Am J Physiol Endocrinol Metab* 2008; 294: E61–E68.
20. Yusta B, Baggio LL, Estall JL, *et al.* GLP-1 receptor activation improves β cell function and survival following induction of endoplasmic reticulum stress. *Cell Metab* 2006; 4: 391–406.
21. Wang J, Takeuchi T, Tanaka S, *et al.* A mutation in the insulin 2 gene induces diabetes with severe pancreatic β-cell dysfunction in the Mody mouse. *J Clin Invest* 1999; 103: 27–37.
22. Stoy J, Edghill EL, Flanagan SE, *et al.* Insulin gene mutations as a cause of permanent neonatal diabetes. *Proc Natl Acad Sci USA* 2007; 104: 15040–15044.
23. Tsunekawa S, Yamamoto N, Tsukamoto K, *et al.* Protection of pancreatic β-cells by exendin-4 may involve the reduction of endoplasmic reticulum stress; *in vivo* and *in vitro* studies. *J Endocrinol* 2007; 193: 65–74.
24. Cunha DA, Ladriere L, Ortis F, *et al.* Glucagon-like peptide-1 agonists protect pancreatic β-cells from lipotoxic endoplasmic reticulum stress through upregulation of BiP and JunB. *Diabetes* 2009; 58: 2851–2862.
25. Butler AE, Janson J, Bonner-Weir S, *et al.* β-cell deficit and increased β-cell apoptosis in humans with type 2 diabetes. *Diabetes* 2003; 52: 102–110.
26. Kendall DM, Riddle MC, Rosenstock J, *et al.* Effects of exenatide (exendin-4) on glycemic control over 30 weeks in patients with type 2 diabetes treated with metformin and a sulfonylurea. *Diabetes Care* 2005; 28: 1083–1091.

Transplant International

Transplant International ISSN 0934-0874

ORIGINAL ARTICLE

Three-dimensional *ex vivo* imaging and analysis of intraportal islet transplants

Hiroyuki Fujimoto,[1] Kentaro Toyoda,[1] Teru Okitsu,[2] Xibao Liu,[1,2] Eri Mukai,[1] Xiaotong Zhuang,[1] Shinji Uemoto,[3] Naoki Mochizuki[4] and Nobuya Inagaki[1,5]

1 Department of Diabetes and Clinical Nutrition, Graduate School of Medicine, Kyoto University, Kyoto, Japan
2 Transplantation Unit, Kyoto University Hospital, Kyoto, Japan
3 Division of Hepato-Pancreato-Biliary Surgery and Transplantation, Department of Surgery, Graduate School of Medicine, Kyoto University, Kyoto, Japan
4 Department of Cell Biology, National Cerebral and Cardiovascular Center Research Institute, Osaka, Japan
5 CREST of Japan Science and Technology Cooperation (JST), Kyoto, Japan

Keywords
allogeneic transplantation, islet transplantation, optical projection tomography, syngeneic transplantation, three-dimensional images.

Correspondence
Nobuya Inagaki, 54 Shogoin Kawahara-cho, Sakyo-ku, Kyoto 606-8507, Japan. Tel.: +81-75-751-3560; fax: +81-75-751-4244; e-mail: inagaki@metab.kuhp.kyoto-u.ac.jp

Conflicts of Interest
All authors have no conflict of interest.

Received: 13 December 2010
Revision requested: 17 January 2011
Accepted: 21 April 2011
Published online: 25 May 2011

doi:10.1111/j.1432-2277.2011.01271.x

Summary

In clinical islet transplantation, because the long-term insulin-independence rate is still poor, a method for detailed analysis of the transplanted islets in the liver after transplantation is required. We have established a novel imaging technique suitable for analysis of transplanted islets in liver using an optical projection tomography (OPT) method. A three-dimensional tomographic image of the transplanted islets in liver was reconstructed. The number of islets transplanted and the number of transplanted islets observed using OPT showed good correlation. The OPT method was used to compare the numbers of transplanted islets in mouse syngeneic and allogeneic transplantation models. Blood glucose concentrations of streptozotocin (STZ)-induced diabetic mice transplanted with syngeneic islets remained normoglycemic and the number of transplanted islets was largely preserved 11 days after transplantation. In mice transplanted with allogeneic islets, hyperglycemia recurred from 7 days after transplantation and the number and the volume of transplanted islets was significantly reduced 11 days after transplantation. These results indicate that OPT imaging and analysis may be a useful tool to quantitatively and sterically evaluation of transplanted islets in liver at the cellular level.

Introduction

Islet transplantation is a promising therapeutic approach for patients with insulin-dependent diabetes mellitus to achieve insulin independence [1,2]. A remarkably high rate of freedom from insulin therapy is achieved in insulin-dependent type 1 diabetic patients after islet transplantation by the Edmonton Protocol [1]. However, it was reported that long-term maintenance of glucose homeostasis without the use of insulin is poor [3]. This decline may be attributed to progressive islet loss as well as to various reactions during and after islet transplantation, including mechanical injury, ischemia, and nonspecific inflammatory reactions [4].

Until now, the total functional volume of islets transplanted intraportally in liver could be monitored only indirectly by measurements such as blood glucose and serum c-peptide levels. Modalities including bioluminescence imaging (BLI) [5–7], magnetic resonance imaging (MRI) [8–11], and positron emission tomography (PET) [12–14] have been used, and transplanted islets were detected by MRI [11] and PET [13] in human. These methods are suitable for *in vivo* examination because they are noninvasive and can be repeated over time. However, islets cannot be evaluated at the cellular level by these methods because the resolution is too low. Conventional immunohistochemical method permit evaluation of beta-cell volume at the subcellular level, but

can only restricted, sliced areas of the sample can be observes. Recently, Hara *et al.* reported subcellular analysis of intact pancreas, but the method can analyze only thin neonatal samples [15]. To investigate engraftment of transplanted islets scattered in solid liver at the subcellular level, another method is required. We have demonstrated an optical projection tomography (OPT) technique for precisely, three-dimensionally evaluating transplanted islets at the cellular level in liver.

Optical projection tomography is a microscopic imaging technique for obtaining three-dimensional, reconstructed images of small biological samples [16]. The principle of OPT is that the light passes through the specimen labeled and cleared for a standard back-projection algorithm to generate a relatively high resolution tomographic image. A three-dimensional image of the specimen is reconstructed using the individual tomographic images. The advantage of OPT is the capability to investigate spatial distribution of such target molecules as RNA and protein without slicing of the target organs and at a higher resolution.

In this report, we show that the number and volume of intraportally transplanted islets in liver can be investigated using OPT analysis. In addition, comparing syngeneic and allogeneic rodent islet transplantation models, we demonstrate that the number and volume of transplanted islets is considerably more decreased in allogeneic islet transplantation than in syngeneic transplantation. Thus, *ex vivo* imaging of intraportal islet transplant using OPT may be a useful tool for evaluation and improvement of islet transplantation outcome.

Materials and methods

Animals

Male C57BL6 Cr Slc mice (Shimizu Laboratory Supplies Co. Ltd, Kyoto, Japan) aged 8–10 weeks were used as recipients and donors and male BALB/c mice (Shimizu Laboratory Supplies Co. Ltd) aged 8 weeks were used as recipients for allogeneic transplantation. All experiments were approved by the Kyoto University Animal Care Committee.

Islet isolation and islet transplantation

Islets were isolated from mouse pancreas using collagenase digestion method [17]; 3–4 ml Hank's Balanced Salt Solution (HBSS) containing 0.5 mg/ml collagenase (Nitta Gelatin, Osaka, Japan) was infused through the common bile duct. The pancreas was dissected and digested at 37 °C for 21 min. Islets were separated from exocrine cells by centrifugation with Ficoll-Conray gradient solution for 10 min. Diabetes was rendered by a single intraperitoneal injection of streptozotocin (STZ) (Nacalai Tesque, Kyoto, Japan), 120 mg/kg body weight, freshly dissolved in 10 mM citrate buffer (pH 4.5). These mice were used as diabetic recipients if the blood glucose concentration was more than 20 mM on two consecutive days. Recipient mice were anesthetized by isoflurane (Forane; Abott, Chicago, IL, USA) during transplantation. Fresh islets in a volume of about 400 μl HBSS were injected into the portal vein and transplanted into the right hepatic lobe as previously reported [18]. For validation of the OPT method, 75, 150 or 300 islets were transplanted into the right hepatic lobe, which was dissected immediately after transplantation. For comparison of syngeneic and allogeneic transplantation, C57BL6 mice ($H\text{-}2^b$) were used as recipients; 300 islets isolated from C57BL6 mice or Balb/c mice ($H\text{-}2^d$) were transplanted, respectively. The blood glucose concentration was determined by glucose meter (Glucocard, Arkley, Japan).

Tissue preparation and immunostaining

Mice with transplanted islets were sacrificed by cervical dislocation. The transplanted right hepatic lobes were dissected clean and immediately immersed for fixation in 4% paraformaldehyde in PBS for 3 h at 4 °C. The fixed samples were washed in PBS and then transferred stepwise to 100% methanol (MeOH) and stored at −20 °C. The immunostaining was performed according to the previous report [19] as follows. The right hepatic lobe was immersed in 15% H_2O_2, 16.7% DMSO solution in MeOH for 24 h to bleach pigmented cells and to reduce auto fluorescence. The liver then was washed in MeOH, which was repeated five times and then kept at −80 °C for at least 1 h before return to room temperature. The organ was rehydrated by Tris Buffered Saline-TritonX (TBST) [0.15 M NaCl (Nacalai Tesque, Kyoto, Japan), 0.1 M Tris (hydroxymethy)aminomethane (Nacalai Tesque, Kyoto, Japan) pH 7.4, and 0.1% Triton X-100 (Nacalai Tesque, Kyoto, Japan)]. TBST containing 10% normal goat serum (Dako Corp., Glostrup, Denmark) and 0.01% sodium azide (Nacalai Tesque, Kyoto, Japan) was used as blocking solution for 24 h. The organ was incubated in insulin antibody (Santa Cruz Biotechnology Inc., Santa Cruz, CA, USA) in 5% DMSO containing blocking solution for 48 h. After washing, Alexa594 goat anti rabbit IgG (Invitrogen, Carlsbad, CA, USA) was used as secondary antibody for 48 h.

Optical projection tomography and image reconstruction

For the observations, the immunostained liver was embedded in 1% agarose gel (low melting point agarose; Sigma Aldrich, St. Louis, MO, USA) to fix the sample.

OPT was performed using an OPT scanner (OPT scanner 3001; Bioptonics, Scotland, UK) according to the manufacturer's instructions [16,19]. The specimens were maintained within the BABB (benzyl alochol/benzyl benzoate 1:2 ratio), rotated to a series of angular positions (0.9° apart) and images were captured at each orientation. High-resolutional tomographic images were reconstructed from raw images by NRecon software (SKYSCAN, Kontich, Belgium). The tomographic images obtained from OPT were reconstructed to three-dimensional form and analyzed by Avizo software (Visualization Science Group, Inc., Burlington, MA, USA). Three-dimensional images of islets and liver were obtained by isosurface treatment. Total volume of all islets was calculated by summation of the selected islets.

Statistical analysis

Data and graph were presented as medians (interquartile range) and statistical analysis was performed with Mann–Whitney's *U*-test. A value of $P < 0.05$ was considered significant.

Results

Observation of transplanted islets in liver by OPT

Transparency of the liver and immunostaining of transplanted islets without sectioning were achieved by the preparation protocols. Figure 1a is a raw OPT image of liver; the insulin-stained transplanted islets are seen as dots in the high magnification image (Fig. 1b, white arrows). One of the tomographic images obtained is shown in Fig. 1c. Vertically reconstructed images are shown in Fig. 1d and e and islets pointed out by arrow and arrowhead in Fig. 1c are located as in Fig. 1d and e, respectively. Some islets appear to be located at the terminal end of the portal vein (Fig. 1c and d) and other islets are located at the wall of the proximal branch of the portal vein (Fig. 1e). Figure 1f is the reconstructed target-specific image of an islet (arrowhead in Fig. 1e) and portal vein. Thus, a three-dimensional image as well as the size and location of transplanted islets in liver can be investigated (Fig. 1g and h and Supplementary movie).

Evaluation of the effectiveness of OPT analysis of transplanted islets in liver

To correlate the number of islets transplanted and the number of islets detected by OPT, we resected and fixed livers immediately after transplantation of a range of numbers of islets. The three-dimensional reconstructed image shows that the number of spots indicating transplanted islets in the right hepatic lobes was increased in accord with the increased dosage (Fig. 2a–c); these numbers are well correlated ($r^2 = 0.9561$) (Fig. 2d). These findings indicate that OPT can be used for quantitative analysis of islets transplanted into liver.

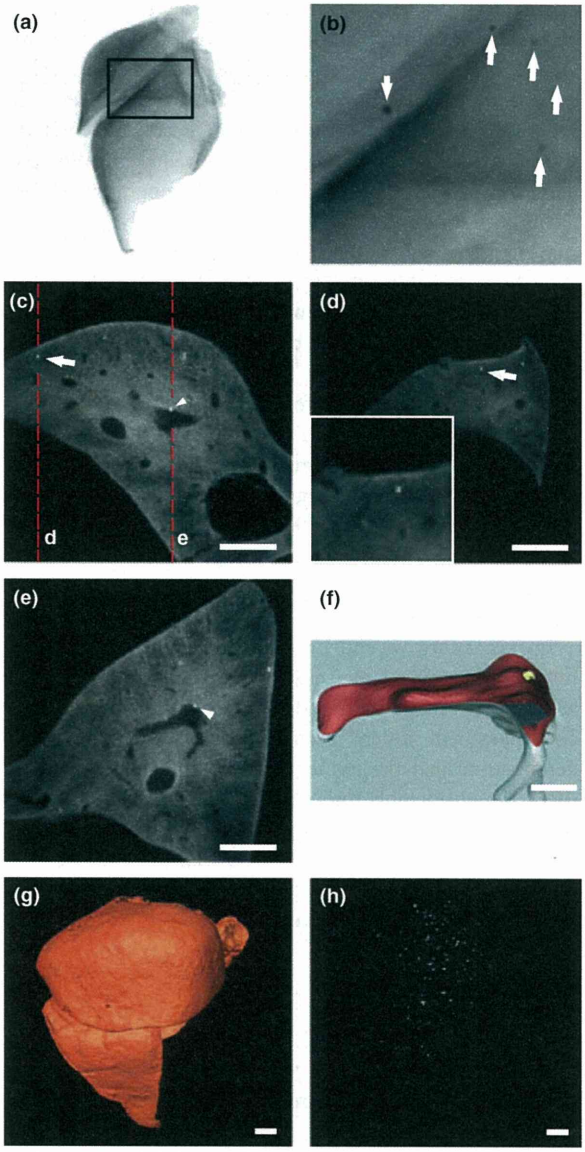

Figure 1 Optical projection tomography (OPT) images of liver containing intraportally transplanted islets. (a) Raw image of islet-transplanted right hepatic lobe, (b) high magnification image [in square of (a)], (c) representative slice image of the transplanted right hepatic lobe; (d and e) vertical slice image of islet with arrow in (c), arrowhead in (c), respectively. (f) Reconstructed three-dimensional image of islet [in (c) and (e), arrowhead] and portal branch. Three-dimensional image of (g) right hepatic lobe; (h) islets (white spots) in liver reconstructed from the same liver sample as (a). Scale bars indicate 1 mm in (c, d, e, g, and h) and 300 μm in (f).

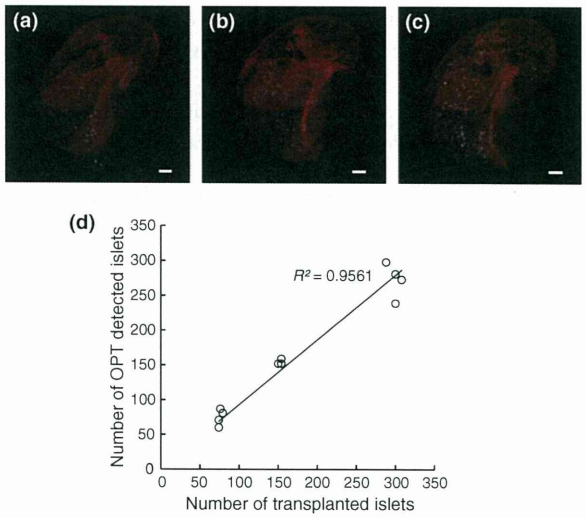

Figure 2 Comparison of the number of islets transplanted with that obtained by optical projection tomography (OPT) analysis. Representative OPT image of recipient liver transplanted with (a) 75, (b) 150, and (c) 300 islets, respectively. (d) Correlation of the number of islets transplanted and OPT-detected islets. Scale bar indicates 1 mm.

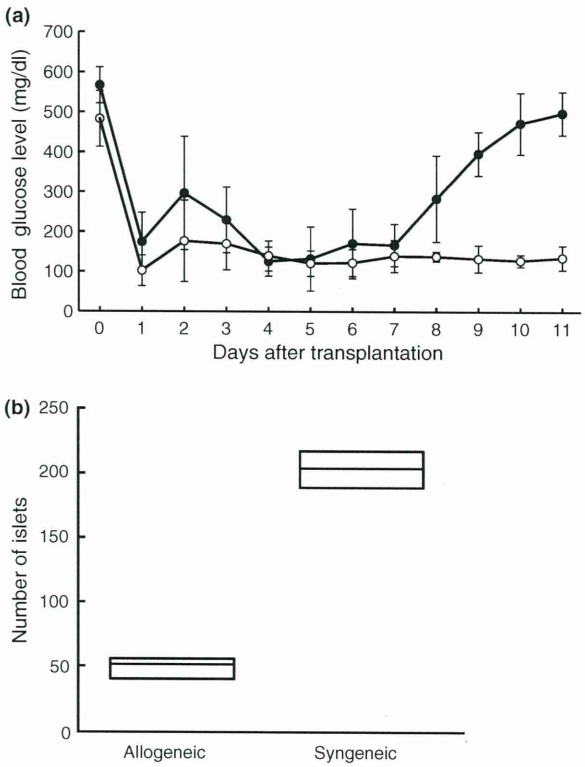

Figure 3 Glycemic level and number of islets of streptozotocin (STZ)-induced diabetic mice after syngeneic and allogeneic islet transplantation. (a) Random blood glucose level of recipients (open circles: syngeneic transplantation, filled circles: allogeneic transplantation). (b) Number of transplanted islets in syngeneic and allogeneic transplantation 11 days after transplantation.

Optical projection tomography analysis of islet grafts under syngeneic and allogeneic conditions

To evaluate the time course of transplanted islets in syngeneic and allogeneic conditions, we analyzed the number and volume of islets intraportally transplanted in liver of STZ-induced diabetic mice. Blood glucose concentrations under both syngeneic and allogeneic conditions were normoglycemic until a week after transplantation. However, blood glucose concentrations under allogeneic conditions thereafter became hyperglycemic, while those under syngeneic conditions remained normoglycemic (Fig. 3a). The islet-containing livers were resected on day 11 for analysis using OPT method. The number of islets in the syngeneic condition was dramatically greater than that in the allogeneic condition [52 (IQR 16.5) vs. 203 (28.5), respectively, $P < 0.05$] (Fig. 3b).

In OPT-detected islets classified by size, the number in each category was significantly greater in syngeneic than in allogeneic conditions and showed a similar histogram pattern (Fig. 4a). Total volume of islets in syngeneic condition was dramatically greater than that in allogeneic condition [8.6 (2.7) vs. 35.3 (10.1) ($\mu m^3 \times 10^6$)], respectively, ($P < 0.05$) (Fig. 4b).

Discussion

In this study, we demonstrate that islets transplanted intraportally in liver can be analyzed at the cellular level using OPT method, which permits three-dimensional analysis of the distribution of the islets in the liver. Comparing syngeneic and allogeneic islet transplantation models, we show by OPT that the volume of transplanted islets differs significantly at the cellular level.

One of main problems in clinical islet transplantation, poor long-term achievement of insulin independence, is primarily attributed to graft loss caused by various stressors upon transplantation [4]. When islets are injected intraportally, each of them is thought to locate at the respective branched end of the portal vein in liver. In modalities such as BLI, MRI, and PET, only PET allows quantification of graft volume, but the resolution is still too low for detailed analysis of the transplanted islets. On the other hand, while the resolution of conventional immunohistochemistry is high, only restricted slices of the engrafted organ can be analyzed using this method.

Optical projection tomography, a newly developed method, is reported to permit analysis of a sample at resolution as high as 5 μm. Recently, Alanentalo *et al.* performed detailed analysis of NOD mice during progression

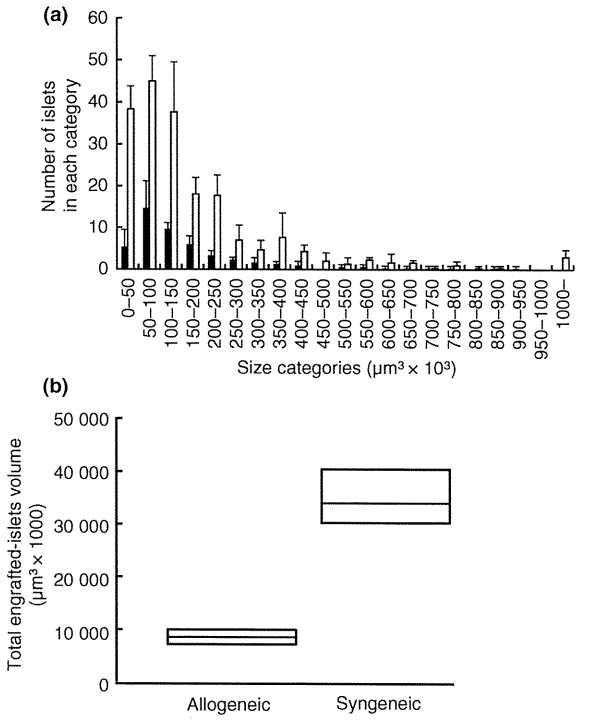

Figure 4 Quantitative analysis of transplanted islets in syngeneic and allogeneic model. (a) Size distribution of transplanted islets. (b) Total volume of transplanted islets in liver obtained using optical projection tomography (OPT) analysis.

of type 1 diabetes and showed that a reduction in volume of native islets in pancreas could be detected and quantified using the OPT method [20]. We have used OPT method for the first time in the intraportal islet transplantation model and confirm the efficacy of this method of islet imaging (Figs 1 and 2).

However, there are several limitations in use of the OPT method. It can be performed only *ex vivo*, and noninvasive, repeated observation is not possible. In this context, PET and MRI are suitable for *in vivo*, repeated monitoring of transplanted islets. In addition, the maximum sample size for analysis using OPT is about 2 cm. The OPT method also is not clinically applicable as it would require a large liver biopsy.

The OPT method is useful for evaluating small organs of small animals such as rodents, as in our present study. Indeed, using rodent islet transplantation models, the OPT method clearly shows quantitative difference of grafts in liver in syngeneic and allogeneic conditions. In this investigation, the OPT method revealed that 83% of the transplanted islets were lost in the allogeneic condition while about 70% were preserved in the syngeneic condition. Moreover, calculated beta-cell volume in the allogeneic condition was significantly reduced to 24.2% of that in the syngeneic condition (Figs 3b and 4b). This remarkable graft loss by allogeneic immune reaction seems not to be related to the size of the islet graft, as there was no difference in size distribution histogram between the two conditions (Fig. 4a). The OPT method also clearly shows the sites where islets adhere and are engrafted in the portal vein. Further investigation is required to determine the effect of islet location on islet engraftment.

In conclusion, we have constructed three-dimensional images of transplanted islets in liver using an OPT method that permits detailed analysis of transplanted islets in liver. This method should be useful for islet transplantation study.

Authorship

HF: designed the study, performed the study, collected the data, analyzed the data, and wrote the paper. KT: designed the study, performed the study, and wrote the paper. TO, SU, and NM: designed the study. XL, EM, and XZ: performed the study. NI: designed the study, wrote the paper.

Funding

This work was supported by a Research Grant from the Ministry of Health, Labour, and Welfare of Japan, and from the Ministry of Education, Culture, Sports, Science, and Technology of Japan, and the Program for Promotion of Fundamental Studies in Health Sciences of the National Institute of Biomedical Innovation (NIBIO), and also by Kyoto University Global COE Program "Center for Frontier Medicine".

Supporting information

Additional Supporting Information may be found in the online version of this article:

Clip S1. Three dimensional image of islets transplanted in liver – Transplanted islets were scattered in liver. This image was reconstructed by software "Avizo".

Please note: Wiley-Blackwell are not responsible for the content or functionality of any supporting materials supplied by the authors. Any queries (other than missing material) should be directed to the corresponding author for the article.

References

1. Shapiro AM, Lakey JR, Ryan EA, *et al.* Islet transplantation in seven patients with type 1 diabetes mellitus using a

glucocorticoid-free immunosuppressive regimen. *N Engl J Med* 2000; **343**: 230.
2. Shapiro AM, Ricordi C, Hering B. Edmonton's islet success has indeed been replicated elsewhere. *Lancet* 2003; **362**: 1242.
3. Ryan EA, Paty BW, Senior PA, *et al.* Five-year follow-up after clinical islet transplantation. *Diabetes* 2005; **54**: 2060.
4. Ricordi C, Strom T. Clinical islet transplantation: advances and immunological challenges. *Nat Rev Immunol* 2004; **4**: 259.
5. Lu Y, Dang H, Middleton B, *et al.* Bioluminescent monitoring of islet graft survival after transplantation. *Mol Ther* 2004; **9**: 428.
6. Fowler M, Virostko J, Chen Z, *et al.* Assessment of pancreatic islet volume after islet transplantation using *in vivo* bioluminescence imaging. *Transplantation* 2005; **79**: 768.
7. Chen X, Zhang X, Larson CS, Baker MS, Kaufman DB. *In vivo* bioluminescence imaging of transplanted islets and early detection of graft rejection. *Transplantation* 2006; **81**: 1421.
8. Evgenov NV, Medarova Z, Guangping D, Bonner-Weir S, Moore A. *In vivo* imaging of islet transplantation. *Nat Med* 2006; **12**: 144.
9. Evgenov NV, Medarova Z, Pratt J, *et al. In vivo* imaging of immune rejection in transplanted pancreatic islets. *Diabetes* 2006; **55**: 2419.
10. Tai JH, Foster P, Rosales A, *et al.* Imaging islets labeled with magnetic nanoparticles at 1.5 Tesla. *Diabetes* 2006; **55**: 2931.
11. Saudek F, Jirák D, Girman P, *et al.* Magnetic resonance imaging of pancreatic islets transplanted into the liver in humans. *Transplantation* 2010; **90**: 1602.
12. Lu Y, Dang H, Middleton B, *et al.* Noninvasive imaging of islet grafts using positron-emission tomography. *Proc Natl Acad Sci USA* 2006; **103**: 11294.
13. Toso C, Zaidi H, Morel P, *et al.* Positron-emission tomography imaging of early events after transplantation of islets of Langerhans. *Transplantation* 2005; **79**: 353.
14. Kim SJ, Doudet DJ, Studenov AR, *et al.* Quantitative micro positron emission tomography (PET) imaging for the *in vivo* determination of pancreatic islet graft survival. *Nat Med* 2006; **12**: 1423.
15. Miller K, Kim A, Kilimnik G, *et al.* Islet formation during the neonatal development in mice. *PLoS ONE* 2009; **4**: e7739.
16. Sharpe J, Ahlgren U, Perry P, *et al.* Optical projection tomography as a tool for 3D microscopy and gene expression studies. *Science* 2002; **296**: 541.
17. Sutton R, Peters M, Mcshane P, Gray DWR, Morris PJ. Isolation of rat pancreatic-islets by ductal injection of collagenase. *Transplantation* 1986; **42**: 689.
18. Yonekawa Y, Okitsu T, Wako K, *et al.* A new mouse model for intraportal islet transplantation with limited hepatic lobe as a graft site. *Transplantation* 2006; **82**: 712.
19. Alanentalo T, Asayesh A, Morrison H, *et al.* Tomographic molecular imaging and 3D quantification within adult mouse organs. *Nat Methods* 2007; **4**: 31.
20. Alanentalo T, Hornblad A, Mayans S, *et al.* Quantification and three-dimensional imaging of the insulitis-induced destruction of β-cells in murine type 1 diabetes. *Diabetes* 2010; **59**: 1756.

Systems analysis of GLP-1 receptor signaling in pancreatic β-cells

Yukari Takeda, Akira Amano, Akinori Noma, Yasuhiko Nakamura, Shimpei Fujimoto and Nobuya Inagaki

Am J Physiol Cell Physiol 301:C792-C803, 2011. First published 6 July 2011;
doi:10.1152/ajpcell.00057.2011

Am J Physiol Cell Physiol 301: C792–C803, 2011.
First published July 6, 2011; doi:10.1152/ajpcell.00057.2011.

Systems analysis of GLP-1 receptor signaling in pancreatic β-cells

Yukari Takeda,[1] Akira Amano,[2] Akinori Noma,[2] Yasuhiko Nakamura,[1] Shimpei Fujimoto,[1] and Nobuya Inagaki[1]

[1]*Department of Diabetes and Clinical Nutrition, Graduate School of Medicine, Kyoto University, Kyoto; and* [2]*Faculty of Bioinformatics, Ritsumeikan University, Kusatsu City, Japan*

Submitted 3 March 2011; accepted in final form 28 June 2011

Takeda Y, Amano A, Noma A, Nakamura Y, Fujimoto S, Inagaki N. Systems analysis of GLP-1 receptor signaling in pancreatic β-cells. *Am J Physiol Cell Physiol* 301: C792–C803, 2011. First published July 6, 2011; doi:10.1152/ajpcell.00057.2011.—Glucagon-like peptide-1 (GLP-1) elevates intracellular concentration of cAMP ([cAMP]) and facilitates glucose-dependent insulin secretion in pancreatic β-cells. There has been much evidence to suggest that multiple key players such as the GLP-1 receptor, G_s protein, adenylate cyclase (AC), phosphodiesterase (PDE), and intracellular Ca^{2+} concentration ($[Ca^{2+}]$) are involved in the regulation of [cAMP]. However, because of complex interactions among these signaling factors, the kinetics of the reaction cascade as well as the activities of ACs and PDEs have not been determined in pancreatic β-cells. We have constructed a minimal mathematical model of GLP-1 receptor signal transduction based on experimental findings obtained mostly in β-cells and insulinoma cell lines. By fitting this theoretical reaction scheme to key experimental records of the GLP-1 response, the parameters determining individual reaction steps were estimated. The model reconstructed satisfactorily the dynamic changes in [cAMP] and predicted the activities of cAMP effectors, protein kinase A (PKA), and cAMP-regulated guanine nucleotide exchange factor [cAMP-GEF or exchange protein directly activated by cAMP (Epac)] during GLP-1 stimulation. The simulations also predicted the presence of two sequential desensitization steps of the GLP1 receptor that occur with fast and very slow reaction rates. The cross talk between glucose- and GLP-1-dependent signal cascades for cAMP synthesis was well reconstructed by integrating the direct regulation of AC and PDE by $[Ca^{2+}]$. To examine robustness of the signaling system in controlling [cAMP], magnitudes of AC and PDE activities were compared in the presence or absence of GLP-1 and/or the PDE inhibitor IBMX.[1]

adenylyl cyclase; glucagon-like peptide-1; model stimulation; phosphodiesterase

UPON ELEVATION of plasma glucose concentration ([glucose]), pancreatic β-cells generate bursts of action potentials to induce cyclic changes in $[Ca^{2+}]$ (55) and regulate pulsatile insulin release (25). This glucose-dependent insulin secretion is synergistically enhanced by incretin hormones, which are released upon meal ingestion from endocrine cells distributed over the intestinal tract (16). The incretin hormones include glucose-dependent insulinotropic peptide (GIP) and glucagon-like peptide-1 (GLP-1). GLP-1 is more effective than GIP to improve deteriorated incretin effect in diabetes and is widely used to treat patients with Type 2 diabetes (45). Elucidation of GLP-1 signaling system in β-cells, therefore, has been an extensive target of experimental studies. To date, it has been well established that GLP-1 activates adenylate cyclases (ACs) through binding to its G protein-coupled receptor and increases [cAMP], the key signal underlying the insulinotropic effects (17, 62).

The [cAMP] is determined primarily by the balance between cAMP production by ACs and degradation by phospodiesterases (PDEs) (8). The activities of several isoforms of AC and PDE expressed in β-cells are controlled by $[Ca^{2+}]$ (11, 28), which is regulated by Ca^{2+}-permeable ion channels and transporters as well as Ca^{2+} release and uptake by the endoplasmic reticulum (ER). The increase in [cAMP] subsequently activates protein kinase A (PKA) and exchange protein directly activated by cAMP (Epac), modulating the activities of multiple ion channels at the plasma membrane (26, 31, 35, 41, 42, 57) and ER (27, 36, 64), which in turn modify the pattern of Ca^{2+} transients. PKA and Epac also have direct effects on proteins that are involved in exocytosis of insulin vesicles (30), and thus the fine regulation of [cAMP] is critical for the adequate insulinotropic effects of GLP-1. However, since multiple signaling factors are involved in regulating [cAMP], the kinetic aspects of the reaction cascade during GLP-1 stimulation have not yet been determined in pancreatic β-cells.

To overcome this difficulty, we developed a mathematical model of GLP-1 receptor signal transduction. We adopted a strategy of estimating individual reaction rates and model parameters by fitting the theoretical reaction scheme to a variety of key experimental findings published to date (3, 11, 54, 66) in both β-cells and insulinoma cell lines. The model thus developed was validated by reconstructing the dynamic changes in [cAMP] during GLP-1 stimulation in the presence and absence of 3-isobutyl-1-methylxanthine (IBMX) observed under various experimental conditions. The model well-simulated GLP-1-induced [cAMP] elevation and predicted the activities of cAMP effectors PKA and Epac as a function of GLP-1. The simulation analysis revealed the presence of two transition steps of receptor desensitization that occur with fast and slow kinetics. The molecular basis for synergistic relationship between glucose and GLP-1 signaling in the cAMP synthesis were clarified by calculating the direct regulation of AC and PDE by $[Ca^{2+}]$. Finally, the robustness of the signaling system in controlling [cAMP] was examined by comparing the AC and PDE activities in the presence or absence of GLP-1 and/or the PDE inhibitor.

Glossary

[L]	GLP-1 (ligand)
[R]	free GLP-1receptor
$[R_t]$	total GLP-1 receptor
$[R_a]$	active GLP-1 receptor
$[R_{D1}]$	desensitized GLP-1 receptor in state 1
$[R_{D2}]$	desensitized GLP-1 receptor in state 2
[LR]	GLP-1 receptor bound with ligand

[1] This article is the topic of an Editorial Focus by Harvey (29a).

Address for reprint requests and other correspondence: N. Inagaki, 54 Shogoin, Kawahara-cho, Sakyo-ku, Kyoto-shi, Kyoto, Japan.

[LRG]	GLP-1 receptor bound with ligand and G_s
[G_t]	total G_s protein
[G]	G_s complex
[$G_{\beta\gamma}$]	β and γ subunit of G_s
[G_αGTP]	total GTP-bound α subunit of G_s
[G_αGDP]	GDP-bound α subunit of G_s
V_{AC_t}	total adenylate cyclase activity
V_C	activity of adenylate cyclase with G protein unbound
$V_{max\_AC\_t}$	Maximum activity of V_{AC}
V_{AC_G}	activity of adenylate cyclase with GαGTP
$V_{max\_AC\_G}$	maximum activity of V_{AC_G}
f_{Cd_AC}	fraction of Ca_xCaM-dependent V_{AC_G}
V_{Cd_AC}	Ca_xCaM-dependent component of V_{AC_G}
[CaM]	Calmodulin
[Ca_xCaM]	Calmodulin bound with Ca^{2+} ions ([Ca_3CaM]+[Ca_4CaM])
[Ca_3CaM]	Calmodulin bound with 3 Ca^{2+} ions
[Ca_4CaM]	Calmodulin bound with 4 Ca^{2+} ions
V_{PDE}	activity of phosphodiesterase
V_{max_PDE}	maximum activity of V_{PDE}
K_{mL}	low K_m of PDE
K_{mH}	high K_m of PDE
f	fraction of PDE with K_{mL}
f_{Cd_PDE}	fraction of Ca_xCaM-dependent V_{PDE}
V_{Cd_PDE}	Ca_xCaM-dependent component of V_{PDE}

METHODS

A minimal model of the GLP-1 receptor signaling transduction in pancreatic β-cells was constructed. Parameters to define the model, including concentrations, binding constants (K_d) of signaling factors, maximum activity (V_{max}) and half-maximal effective concentration ($K_{1/2}$) of substances for activation of enzymes, rate constants, and various magnitude factors of kinetic equations are listed in APPENDIX I. The time-based integration of six differential equations (*Eqs. 3–8*) were performed using the Euler method with a time step of <2 ms on the Microsoft Visual Studio platform. The units of time and substrate concentrations are secons and millimolar (indicated otherwise), respectively.

Activation of GLP-1 receptor. Figure 1 shows the reaction scheme of the minimal model of the GLP-1 receptor cascade. Active receptors may form three different conformations: free receptor (R), ligand (L)-bound receptor (LR), and the Gs-bound LR complex (LRG). Binding reactions indicated by black arrows were assumed to be much faster than the rest of reactions associated with conformational changes (22), and thus an instantaneous equilibrium was assumed for the reactions enclosed within the red rectangle. The dissociation constant (K_d) for GLP-1 binding to the receptor has been determined in expression systems (43, 65), whereas K_d for LR and G was estimated by fitting the [GLP-1]-dependent [cAMP] accumulation (66). In calculating the reaction cascade, total amounts [R_t] and [G_t] were conserved by applying *Eqs. 1* and *2*, respectively.

$$[R_t] = [R_a] + [R_{D1}] + [R_{D2}] \quad \text{Where } [R_a] = [R] + [LR] + [LRG]. \tag{1}$$

$$[G_t] = [G_{\alpha\beta\gamma}] + [G_{\beta\gamma}] \quad \text{Where } [G_{\alpha\beta\gamma}] = [G] + [LRG] \tag{2}$$

Upon ligand binding, the GLP-1 receptor undergoes desensitization through phosphorylation by unknown mechanisms (67). Although the molecular mechanism has not been elucidated, the computer simulation of the spontaneous decay in [cAMP] during continuous stimulation with GLP-1 (see Fig. 3) as well as desensitized [cAMP] production after preconditioning of GLP-1 receptors (see Fig. 4) suggested the presence of two sequential desensitization states R_{D1} and R_{D2}. We assume that the first desensitization step to R_{D1} occurs from the ligand-bound form of the receptor, (LR + LRG), followed by the second transition to R_{D2} with a recovery steps to R_a (see Fig. 1). The rate constants for the time-dependent desensitization were determined by fitting the kinetic sheme to experimental recordings, and the time-dependent changes in [R_{D1}] and [R_{D2}] are defined with *Eqs. 3* and *4*, respectively.

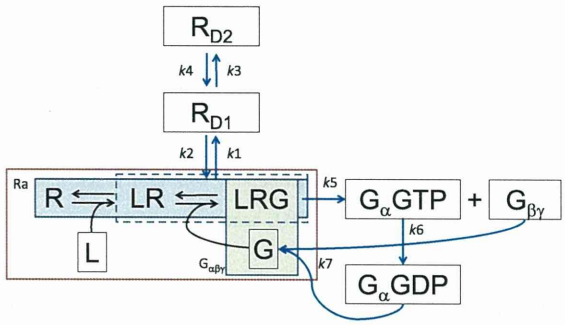

Fig. 1. Reaction scheme of glucagon-like peptide-1 (GLP-1) receptor activation. The receptor takes five different conformations: R, free receptor; LR, ligand (L)-bound form; LRG, G_s-bound LR complex; R_{D1}, desensitized receptor at the state D1 with faster kinetics defined by rate constants *k*1 and *k*2; and R_{D2}, desensitized receptor at the state D2 with the very slow kinetics defined by rate constants *k*3 and *k*4. The desensitization to R_{D1} occurs only from the ligand bound form (LR and LRG) with *k*1, and the recovery to active receptos (R_a) (= R + LR + LRG) with *k*2. States of G_s protein include $G_{\alpha\beta\gamma}$, heterotrimeric complex (for [G] and [LRG]) and dissociated subunits G_αGTP, G_αGDP, and $G_{\beta\gamma}$. Time-dependent changes in conformations of G protein are calculated by rate constants of G_s dissociation into G_αGTP and $G_{\beta\gamma}$ subunits (*k*5), subsequent hydrolysis of GTP (*k*6), and reassociation of G_αGDP with $G_{\beta\gamma}$ (*k*7). The reaction steps marked with a black arrow were calculated assuming instantaneous equilibrium, whereas those marked with blue arrows were calculated by the time-based integration using the Euler method. When calculating the instantaneous equilibrium enclosed with the red rectangle, the constraint of mass conservation was applied to the sum of (R + LR + LRG) and (G + LRG), respectively, at each time step.

$$d[R_{D1}]/dt = k1 \cdot ([LR] + [LRG]) - k2 \cdot [R_{D1}] - k3 \cdot [R_{D1}] + k4 \cdot [R_{D2}] \tag{3}$$

$$d[R_{D2}]/dt = k3 \cdot [R_{D1}] - k4 \cdot [R_{D2}] \tag{4}$$

The kinetics for the activation and deactivation of G protein are calculated by rate constants of G dissociation into G_αGTP and $G_{\beta\gamma}$ subunits and subsequent hydrolysis of GTP (APPENDIX I), which have been biochemically investigated (5, 56). The time-dependent changes in [G_αGTP], [G_αGDP], and [$G_{\beta\gamma}$] are described by the following differential equations:

$$d[G_\alpha GTP]/dt = k5 \cdot [LRG] - k6 \cdot [G_\alpha GTP] \tag{5}$$

$$d[G_\alpha GDP]/dt = k6 \cdot [G_\alpha GTP] - k7 \cdot [G_\alpha GDP] \cdot [G_{\beta\gamma}] \tag{6}$$

$$d[G_{\beta\gamma}]/dt = k5 \cdot [LRG] - k7 \cdot [G_\alpha GDP] \cdot [G_{\beta\gamma}] \tag{7}$$

AC and PDE activities. The level of [cAMP] is determined by the balance between production rate (V_{AC_t}) and degradation rate (V_{PDE}) by ACs and PDEs, respectively (*Eq. 8*).

$$\frac{d[cAMP]}{dt} = V_{AC\_t} - V_{PDE} \tag{8}$$

At least nine different isoforms of membrane-bound AC have been identified (29). In pancreatic β-cells, ACVIII was suggested to play a predominant role in synthesis of cAMP during GLP-1 stimulation of β-cells (53). The modulation of ACVIII by both Ca^{2+}-bound calmodulin (Ca_xCaM) and $G_{s\alpha}$GTP would provide the molecular basis for synergistic relationship between glucose and GLP-1 stimulation in the cAMP synthesis (11). In addition to this adaptable component

(V_{AC_G}), a basal component (V_{AC}) was assumed to maintain the resting [cAMP] in the absence of agonists. Thus the total activity of ACs (V_{AC_t}) is given by a sum of V_{AC} and V_{AC_G} (*Eqs. 9–11*).

$$V_{AC\_t} = V_{AC} + V_{AC\_G} \quad (9)$$

$$V_{AC} = V_{max\_AC} \cdot \frac{0.0004}{0.0004 + G_\alpha GTP} \cdot \frac{[ATP]}{[ATP] + 1.03} \quad (10)$$

$$V_{AC\_G} = V_{max\_AC\_G} \cdot \frac{G_\alpha GTP}{0.0004 + G_\alpha GTP} \cdot \frac{[ATP]}{[ATP] + 0.315} \times \left((1 - f_{Cd\_AC}) + f_{Cd\_AC} \cdot \frac{[Ca_3CaM] + [Ca_4CaM]}{[Ca_3CaM] + [Ca_4CaM] + 0.000348} \times \frac{0.075}{0.075 + [Ca^{2+}]} \right) \quad (11)$$

The $G_\alpha GTP$-dependent activation of AC was calculated with a $K_{1/2}$ determined by Sunahara and colleagues (58). An [ATP] of 3 mM was used in the present study, and the $K_{1/2}$ of [ATP] defining the substrate dependency of V_{AC} and V_{AC_G} were adopted from Dessauer et al. (13). The term for Ca^{2+}-dependent regulation of V_{AC_G} in *Eq. 11* was originally developed in *Aplysia* neurons (69) and was modified to fit the ACVIII activity (21) in the β-cell model by Fridlyand et al. (23). *Eq. 11* contains both Ca_xCaM ([Ca_3CaM]+[Ca_4CaM])-mediated activation and Ca^{2+}-dependent inhibition. We additionally introduced f_{Cd_AC}, the fraction of Ca_xCaM-dependent V_{AC_G}. A [Ca^{2+}] of 500 nM was assumed under a high-glucose condition and a resting [Ca^{2+}] of 100 nM for a lower glucose concentration used in experiments (18, 33, 60). An instantaneous equilibrium was assumed for the binding of Ca^{2+} to CaM using the association and dissociation rate constants given by Yu and colleagues (69). The V_{AC_t} was determined at 1.8 μM/s from the initial rate of rise (dashed line in Fig. 3*A*) of [cAMP] evoked by GLP-1 in the presence of high [IBMX] > 250 μM and [glucose] > 20 mM. Based on this estimation, V_{max} of AC activities (V_{max_AC} and $V_{max\_AC\_G}$) and fractions (f) of the Ca^{2+}-dependent component of V_{AC_G}(f_{Cd_AC}) were optimized (see APPENDIX I) by reconstructing experimental findings with the whole reaction scheme.

In β-cells, it has been suggested that several PDE isoforms (1C, 3B, 4, 8B, and 10A) are involved in regulation of insulin secretion (15, 51). However, the fractional contribution of each isoform to cAMP degradation in intact cells has not yet been determined. Sams and Montague (54) observed over 70% of total PDE activity in the supernatant fraction of an homogenate of islets of Langerhans. Their kinetic analysis of the soluble PDEs suggested the presence of at least two fractions with different activities, as indicated by two linear components (dashed and solid black lines) in the Lineweaver-Burk plot (Fig. 2). We reevaluated the experimental results by fitting the data with a sum of two Michaelis-Menten functions (*Eq. 12*) in the present study.

$$V_{PDE} = V_{max\_PDE} \cdot \left(\frac{f \cdot [cAMP]}{[cAMP] + K_{mL}} + \frac{(1 - f) \cdot [cAMP]}{[cAMP_f] + K_{mH}} \right) \quad (12)$$

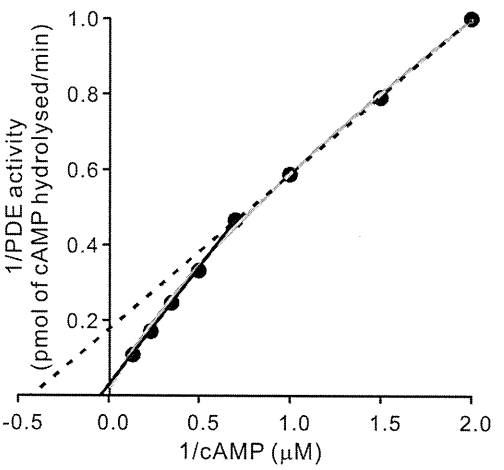

Fig. 2. Determination of K_m values of phosphodiesterase (PDE) based on experimental Lineweaver-Burk plots. Filled circles and fitted (dotted and black) lines are reproduction of experimental data (54) determined in guinea pig islets. The properties of the PDE activity components were reevaluated by fitting the experimental results with *Eq. 12* (solid gray line).

The fitting (gray curve in Fig. 2) determined the K_m values (K_{mL} and K_{mH}) and f of the two components. V_{PDE} thus reflects the sum of all PDE activities.

Since Ca_xCaM-sensitive PDE1C plays a functional role in degradation of cAMP in the β-cell lines βTC3 (28) and MIN6 (38), a Ca^{2+}-dependent component was added to the PDE model (*Eq. 13*).

$$V_{PDE} = V_{max\_PDE} \cdot \left(\frac{f \cdot [cAMP]}{[cAMP] + K_{mL}} + \frac{(1 - f) \cdot [cAMP]}{[cAMP] + K_{mH}} \right) \left[(1 - f_{Cd\_PDE}) + f_{Cd\_PDE} \cdot \frac{[Ca_3CaM] + [Ca_4CaM]}{[Ca_3CaM] + [Ca_4CaM] + 0.000348} \right] \quad (13)$$

The half-maximal value of Ca_xCaM for the stimulation of PDE (68) was adopted from the PDE model developed for β-cells (23), and f_{Cd_PDE} reflects the fraction of the Ca_xCaM-dependent component of the enzyme. Given the [cAMP]s determined under various experimental conditions (Table 1), V_{max_PDE} and f_{Cd_PDE} (APPENDIX I) were finely adjusted by reconstructing these experimental findings using 100 or 500 nM [Ca^{2+}] according to the [glucose] used in experiments.

In experimental studies, the rise in [cAMP] evoked by GLP-1 saturates even in the presence of a maximal inhibitory concentration of IBMX, indicating that some fraction of PDE activity still remained, controlling [cAMP]. Ahmad and colleagues (1) showed that ~80% of the soluble PDE activity in a β-cell line (BRIN-BD11 cells) was blocked by [IBMX] > 200 μM, and thus we assumed that the

Table 1. *Comparison of [cAMP] between experimental measurements in rat primary pancreatic β-cells and model simulations under control conditions and after 15 min stimulation with GLP-1 with or without IBMX*

	Experimental Data	Simulation Result	Experimental Data	Simulation Result
Experimental conditions:	1.4 mM Glucose	100 nM Ca^{2+}	20 mM Glucose	500 nM Ca^{2+}
cAMP levels, μM				
Resting (control)	3.4	1.6	3.2	1.4
10 nM GLP-1		4.2		5.6
Resting w/ IBMX	10.5	12.0	11.7	10.3
10 nM GLP-1w/ IBMX	38.2	37.0	55.2	57.6

The cAMP levels were indicated in units of fmol·10^3 cells^{-1} in the experimental work (11), and we converted these units to μM by assuming the cytoplasmic volume of a single β-cell [764 fL; (10)]. Administration of IBMX (250 μM) was simulated by decreasing PDE activity by 80%. See text for definitions of abbreviations.

IBMX-insensitive PDE8 may contribute 20% PDE activity in the presence of a high [IBMX].

PKA and Epac activities. Although pancreatic β-cells most likely express both PKA type I and II (2, 37, 39), the isoform predominantly regulating the insulinotropic effect of GLP-1 has not been investigated. Since K_d of PKA type I [2.9 μM (9)] and the half-maximal [cAMP] for the activation of type II [$K_{1/2}$ = 2~3 μM (7)] were very similar, we included one hypothetical type of PKA in the present model, and the activity was calculated with a K_d of 2.9 μM (Hill coefficient, n_H = 1.4) determined by Dao et al. (9). Distinct values of $K_{1/2}$ were reported for Epac1 and 2 [30 μM for Epac1 (20) and 20 μM for Epac2 (52, 63)], and thus the active fractions were separately determined.

RESULTS

[cAMP] in pancreatic β-cells under resting conditions and GLP-1 stimulation. The basal level of [cAMP] was 1.6 μM at 100 nM [Ca^{2+}] and 1.4 μM at 500 nM [Ca^{2+}] in our model simulation (Table 1). These values of [cAMP] are comparable to 3.4 and 3.2 μM measured in rat primary β-cells at 1.4 and 20 mM [glucose], respectively (11). Upon stimulation with 10 nM GLP-1 for 15 min, [cAMP] increased to 4.2 μM at 100 nM [Ca^{2+}] and to 5.6 μM at 500 nM [Ca^{2+}] in our model. If PDE was inhibited by 80% (corresponding to 250 μM IBMX) in the absence of GLP-1, [cAMP] increased to ~11 μM independently of [Ca^{2+}] levels. These results also agreed well with the experimental observations. When stimulated with 10 nM GLP-1 in the presence of IBMX, [cAMP] elevated to 37.0 μM at 100 nM [Ca^{2+}] and further to 57.6 μM at 500 nM [Ca^{2+}], similarly to the experimental records of 38.2 and 55.2 μM obtained at the low (1.4 mM) and high (20 mM) [glucose], respectively.

The experimental time course of [cAMP] accumulation induced by GLP-1 (66) was also examined (Fig. 3). Upon stimulation with GLP-1 at 25 mM [glucose] in the presence of IBMX, [cAMP] increased rapidly and slowly declined after reaching peaks within 4 min (filled circles, Fig. 3*A*). The time course of [cAMP] was well reconstructed by simulation at 20% PDE activity and 500 nM [Ca^{2+}] (black curve, Fig. 3*A*). The velocity of cAMP degradation by PDE gradually increases with increasing [cAMP], and the peak is attained when the production rate of cAMP (V_{AC_t}) matched the degradation rate by PDE (V_{PDE} in *Eq. 8*). Simulations revealed that the time to peak as well as the subsequent slow decline in [cAMP] were also influenced by desensitization of the GLP-1 receptor, predominantly due to the state transition to R_{D1} (Fig. 1). In the absence of IBMX, the balance between AC and PDE activities are attained at a much lower [cAMP], thereby giving a time to peak of <1 min (gray curve, Fig. 3*A*). The simulation result was also in good agreement with experimental data (open circles, Fig. 3*A*).

The experimental dose-response relationship obtained by Widmann and colleagues (66) was reconstructed by calculating the [cAMP] accumulation attained over 10 min application of different concentrations of GLP-1 at 20% PDE activity and 500 nM [Ca^{2+}] (Fig. 3, *B* and *C*). At 0.001 and 0.01 nM [GLP-1], [cAMP] increased to a stable saturation level within 2 min (Fig. 3*B*), whereas at higher [GLP-1], the time to peak was delayed with increasing [GLP-1] and the desensitization became more pronounced. As [GLP-1] increases, the activation of V_{AC_G} (see *Eqs. 9~11*) became significant when [GLP-1] >

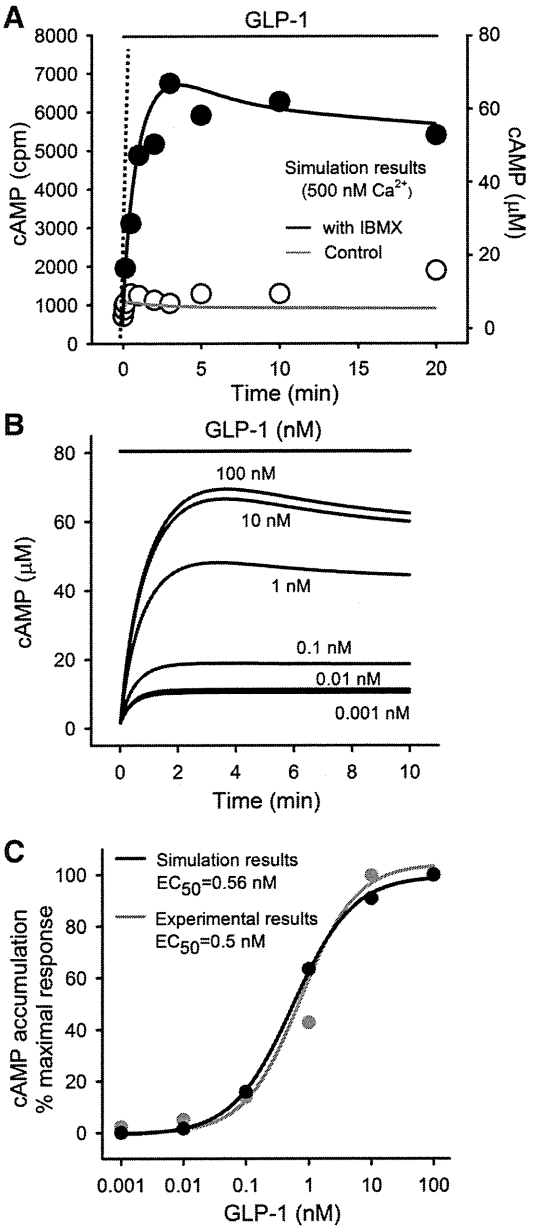

Fig. 3. Time courses of [cAMP] change induced by applying 100 nM GLP-1 (indicated by a horizontal line at the top). *A*: open circles (control) and filled circles [with 1 mM 3-isobutyl-1-methylxanthine (IBMX)] are reproduction of experimental data (66) obtained at 25 mM [glucose] in INS-1 cells. For conversion of units on the left to right vertical axes, see the legend of Table 1. The black and gray curves are simulation results at 500 nM [Ca^{2+}] with and without IBMX, respectively. A 20% activity of PDE was assumed in the presence of IBMX. The dotted line was fitted to the initial rate of rise of [cAMP] to determine the activity of adenylate cyclase (AC). *B*: simulated time courses of the dose-dependent [cAMP] accumulation at 500 nM [Ca^{2+}] during continuous GLP-1 stimulation under the presumptive presence of IBMX (PDE activity inhibited by 80%). *C*: [cAMP] responses to 10 min stimulation with GLP-1 expressed as the percentage of the maximal response in simulation (black line). The dose-response curve was compared with that measured in INS-1 cells (grey line) (66).

0.1 nM and nearly saturated at [GLP-1] slightly larger than 10 nM. In Fig. 3*C*, the dose-dependent accumulation of cAMP at the end of 10 min application of different concentrations of GLP-1 are compared between the simulation and experimental

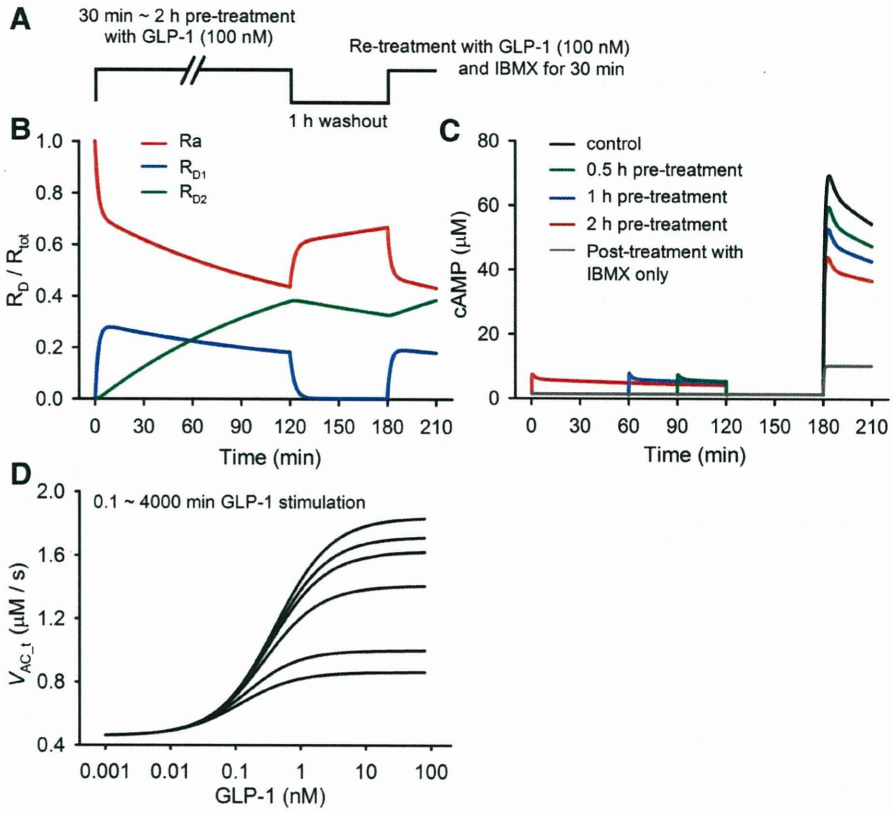

Fig. 4. GLP-1 receptor desensitization. *A*: protocol used in the experimental study of receptor desensitization (3). GLP-1 at 100 nM was applied for various conditioning periods of 30 min to 2 h followed by a 1-h pause before the test application of the same dose. IBMX was only applied with the second application of GLP-1. *B*: time course of the probability of R_a (red) and those of R_{D1} (blue) and R_{D2} (green) in response to the 2-h pretreatment protocol. *C*: [cAMP] response (at 500 nM [Ca^{2+}]) to the experimental protocol with varying pretreatment periods, indicated by different colors. The gray trace was obtained by applying IBMX only at the time point of 180 min. *D*: [GLP-1] − V_{AC_t} relations at the end of different stimulation periods of 6 s, 10 s, and 1, 2, 20, 200, 2,000, and 4,000 min, from *top* to *bottom* of 8 curves, respectively. The traces of 6 and 10 s stimulation almost overlapped with one another, indicating that the desensitization was invisible with these short periods, whereas traces with 2,000 and 4,000 min stimulation also overlapped, indicating saturation of the desensitization already at ~2,000 min.

results in INS-1 cells. The half-maximal [GLP-1] is 0.56 nM in the simulation, which is only slightly larger than that obtained in INS-1 cells (0.50 nM).

Ultra-slow desensitization of the GLP-1 receptor. The simulation analysis suggested that the gradual decay of [cAMP] after the peak (Fig. 3, *A* and *B*) during GLP-1 stimulation largely reflects desensitization of the ligand-bound receptor (LR and LRG in Fig. 1) to R_{D1}. However, the R_{D1} kinetics alone failed to reconstruct the very slow inactivation remaining 1 h after washing out agonist as observed by Baggio and colleagues (3). The model including an R_{D2} state in series with R_{D1} reconstructed well the desensitization phenomenon in response to the experimental protocol (Fig. 4*A*). When the 2-h prestimulation protocol was applied (Fig. 4*B*), the R_{D1} fraction (blue curve) increased to a maximum of ~0.28 at the expense of the active fraction (R_a, red curve) within the initial 10 min, and then both R_a and R_{D1} slowly declined thereafter due to a continuous transition to R_{D2} (green curve). During the washout period, the R_{D1} fraction quickly became insignificant, whereas 85% of R_{D2} remained even after 1 h washout. The result suggests that the fraction of R_a available for the second application of GLP-1 decreases depending on the preincubation period. Figure 4*C* shows the [cAMP] response to the experimental protocol with varying pretreatment periods. It is evident, as predicted, that the longer the preincubation period, the more the [cAMP] response was reduced on the second application of GLP-1. The reductions (in %) in [cAMP] accumulations on the second stimulus were normalized to the control amplitude and were summarized in Table 2. These results agreed well with the experimental observations (3).

To characterize the steady-state desensitization of the GLP-1 receptor, the [GLP-1]-dependent V_{AC_t} at varying incubation periods (10 s ~ 4,000 min) were computed over the range 0.001~100 nM [GLP-1] (Fig. 4*D*). With 6- and 10-s applications, V_{AC_t} nearly overlap one another virtually without any sign of receptor desensitization. When the duration of GLP-1 application was prolonged, the desensitization gradually developed and a steady state was obtained at ~2,000 min application, which gave ~25% of the control V_{AC_t} at the saturating [GLP-1]. The extent of desensitization was more pronounced when stimulated with higher [GLP-1].

Cross-talk between glucose and GLP-1 signal pathways in determining [cAMP]. Experimental studies in Min6 and INS-1 β-cells demonstrated that [cAMP] increased in phase with a temporal increase in [Ca^{2+}] in the presence of GLP-1, whereas

Table 2. *Reduction of GLP-1-dependent [cAMP] accumulation induced by prestimulation of receptors for different time periods*

	Preincubation Period With 100 nM GLP-1		
	0.5 h	1 h	2 h
% Reduction			
Simulation results	16	26	40
Experimental results	21	35	50

The [cAMP] accumulation caused by IBMX alone (Fig. 4*C*) was subtracted from the [cAMP] responses to the second application of agonist, and the differences were normalized to the control value. The simulation results are compared with the experimental data in INS-1 cells (3). See text for definitions of abbreviations.